Acta Crystallographica Section D
Biological Crystallography
ISSN 0907-4449

Using a quasi-parallel X-ray beam of ultrashort wavelength for high-pressure virus crystallography: implications for standard macromolecular crystallography

Roger Fourme,[a]* Éric Girard,[a] Richard Kahn,[b] Isabella Ascone,[c] Mohamed Mezouar,[d] Anne-Claire Dhaussy,[d] Tianwei Lin[e] and John E. Johnson[e]

[a]Synchrotron SOLEIL, BP48 Saint Aubin, 91192 Gif sur Yvette, France, [b]IBS, 41 Rue Jules Horowitz, 38027 Grenoble CEDEX, France, [c]LURE, Bâtiment 209D, Université Paris-Sud, 91898 Orsay CEDEX, France, [d]ESRF, BP220, 38027 Grenoble CEDEX, France, and [e]Department of Molecular Biology, The Scripps Research Institute, 10550 North Torrey Pines Road, La Jolla, CA 92037, USA

Correspondence e-mail: roger.fourme@synchrotron-soleil.fr

Received 30 April 2003
Accepted 23 July 2003

Data acquisition from crystals of an icosahedral virus, cowpea mosaic virus (CPMV), was carried out to 2.8 Å resolution under an elevated hydrostatic pressure of 330 MPa. This was the first example of a complex macromolecular assembly to be studied by high-pressure crystallography. The data were obtained from the ESRF ID30 beamline using a quasi-plane wave of ultrashort wavelength with a diamond anvil cell and an imaging-plate detector. The results of the high-pressure data analysis are given and are compared with those obtained under standard conditions, showing that the experimental procedures implemented are very efficient in terms of diffraction information collected per unit volume of crystal. These results suggest that the use of a quasi-parallel synchrotron radiation beam of ultrashort wavelength should also be considered for conventional macromolecular crystallography data collection.

1. Introduction

The first X-ray crystallographic study of a protein, hen egg-white lysozyme (HEWL), under high pressure was carried out by Kundrot & Richards (1987). A beryllium cell was employed to produce the pressure of 100 MPa (Kundrot & Richards, 1986). A similar device was also used to study sperm whale myoglobin at 150 MPa (Urayama *et al.*, 2002). There are several drawbacks associated with this type of high-pressure cell: (i) no optical observation can be performed, (ii) polycrystalline beryllium produces powder diffraction and diffuse scattering and (iii) the pressure is limited to 200 MPa. The diamond anvil cell (DAC; Weir *et al.*, 1959) with the metal gasket technique for encapsulating the sample (Van Valkenburg, 1962) opened up new possibilities. The compressibility of lysozyme at pressures as high as 1 GPa was determined using DAC and short-wavelength[1] X-rays from synchrotron radiation (Katrusiak & Dauter, 1996) without subsequent data collection.

We exploited the application of X-rays of ultrashort wavelength to macromolecular crystallography at high pressure with a DAC at room temperature. Experiments were performed on the ID30 high-pressure beamline at the ESRF, initially on protein crystals (Fourme *et al.*, 2001). We then demonstrated the feasibility of high-pressure crystallography on a complex macromolecular assembly, the capsid of cowpea mosaic virus (CPMV; Fourme *et al.*, 2002). In subsequent experiments, we have collected a high-completeness 2.8 Å data set for cubic CPMV crystals at 330 MPa. In this report, we present the experimental procedures which were used to

[1] Short, very short and ultrashort wavelengths are close to 0.9, 0.5 and 0.3 Å, respectively (nomenclature from Helliwell *et al.*, 1993).

overcome the constraints of high-pressure containment and we report results of the data collection at 330 MPa. On this basis, we suggest that some procedures that were initially developed for high-pressure crystallography should also be considered for standard (*e.g.* atmospheric pressure) macromolecular crystallography.

2. Materials and methods

There are several experimental constraints imposed by the use of the DAC. (i) The angular apertures of the DAC for both incident and diffracted rays are limited. 53° is the largest angular aperture that could be exploited in our experiments with 1 mm thick diamond anvils. With thinner diamonds, the aperture has now been increased to about 90°. (ii) Hydrostatic compression must be maintained during the experiment, which precludes the use of cryo-temperatures to increase the sample lifetime. On the other hand, there will be no increase in mosaicity owing to flash-cooling. Our previous experience shows that high pressure can also help in maintaining low mosaicity. (iii) The small chamber of the DAC limits the size of crystals that can be used. Additionally, the diamonds absorb and scatter radiation. Therefore, it is important to optimize the diffraction signal-to-background noise ratio. (iv) X-ray absorption by diamond anvils is a source of systematic errors in high-pressure data collection. We take steps to relieve these constraints in the experimental setup.

2.1. Source, X-ray beam and wavelength

It can be argued that the optimal X-ray beam for high-pressure experiments is a quasi-plane wave (*i.e.* a beam with very low divergence and small $\delta\lambda/\lambda$) of ultrashort wavelength and very high intensity. The final choice of the wavelength is related to the particular detector used.

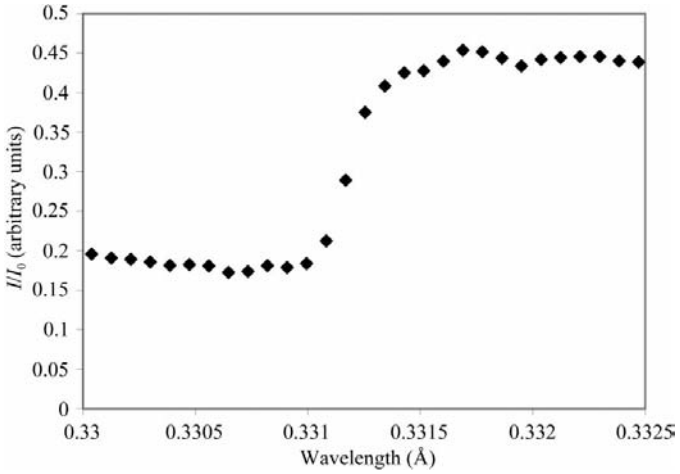

Figure 1
Transmission of a piece of imaging plate in the wavelength domain around the Ba *K* absorption edge recorded in the ID30 experiment. Monochromator and beam characteristics were as in the high-pressure data collection on CPMV. The transmission is expressed on a relative scale, as I and I_0 were measured with two different diodes.

2.1.1. Ultrashort wavelength. The use of ultrashort wavelengths for protein crystallography experiments was first advocated by Helliwell & Fourme (1983). The potential benefits of using short-wavelength X-rays for protein crystallography were examined by Arndt (1984). Helliwell *et al.* (1993) have demonstrated the feasibility of collecting data frames from a HEWL crystal at wavelengths of 0.5 and 0.3 Å. Gonzalez *et al.* (1994) compared the quality of data and the relative background level in diffraction patterns obtained from a HEWL crystal at wavelengths of 0.92 and 0.55 Å. The first fully documented report of a complete protein crystallography experiment at ultrashort wavelength (0.358 Å, at the Xe *K* absorption edge), from data collection to the calculation of an electron-density map, was provided by Schiltz *et al.* (1997). This experiment acquainted some of us with the use of ultrashort wavelengths, which were of obvious potential interest for high-pressure experiments. The absorption of X-rays by diamond decreases at shorter wavelengths, but Compton scattering increases rapidly below 0.4 Å. Accordingly, the wavelength range between 0.3 and 0.4 Å is the natural choice for experiments with the DAC. The low Bragg angles of diffraction from such wavelengths is compatible with the limited apertures of the DAC. As the diffraction is nearly normal to the detector surface, limiting the extension of Bragg reflections, the signal-to-noise ratio will also be improved.

The X-ray wavelength actually used in our experiments was selected taking into account the particular detector used (MAR 345), which was based on an imaging plate (ST5 from Fuji). The sensitive layer of the imaging plate contains $BaFBr:Eu^{2+}$ and the stopping power and hence the DQE (detective quantum efficiency) in the 0.3–0.4 Å wavelength range essentially depends on the absorption coefficient of the heaviest element, barium (Helliwell, 1992). The selected wavelength was 0.3310 Å, at the beginning of the high-energy plateau of the absorption spectrum of Ba around the *K* edge (Fig. 1). The energy shift of Compton-scattered photons is proportional to d^{-2}, where d is the crystallographic resolution (Fourme *et al.*, 2001). At the selected wavelength, the DQE of

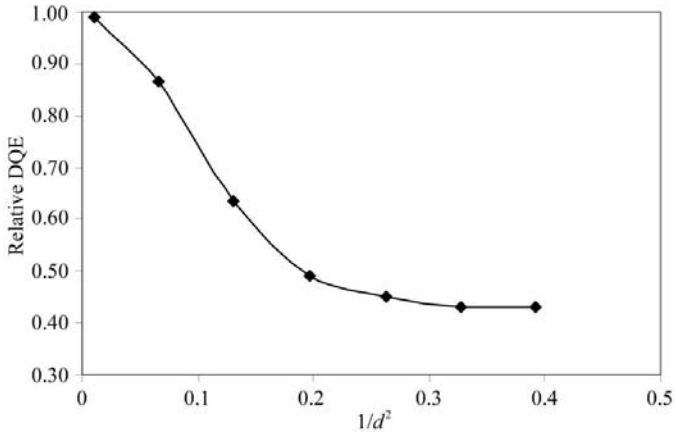

Figure 2
Relative variation as a function of $1/d^2$ of the DQE of the imaging plate for Compton scattering produced by an X-ray beam of wavelength 0.3310 Å, based on data in Fig. 1.

the detector is maximal for elastic scattering and reduced for Compton scattering. The reduction is resolution-dependent and the correlated gain in the signal-to-noise ratio is quite substantial (>2) at high resolution (Fig. 2).

At 0.331 Å, the sample transmission is ∼99%. The linear absorption coefficient of diamond at this wavelength is 0.0756 mm^{-1}, so the transmission through a 1 mm thick diamond plate is 92.7 and 91.9% for beams inclined by 0 and 26.5°, respectively, with respect to the DAC axis. The transmission of the incoming X-ray beam through the lower diamond anvil is constant for each frame and varies gradually from frame to frame as the DAC is rotated during data collection; the corresponding (small) variations are taken into account efficiently by the scaling procedure. The transmission of diffracted beams through the upper diamond anvil varies by 0.9% from the shortest to the longest path lengths and the average variation is lower; therefore, no absorption correction was applied. With the increase in the cell aperture from 53 to about 90° in our latest design, relative variations are larger (∼3%) and systematic absorption correction based on path-length calculations would then be worthwhile for very accurate data collection.

The wavelength-dependent radiation damage requires investigation under non-cryogenic conditions. Crystal lifetime is improved by employing short wavelengths rather than Cu $K\alpha$ radiation (Helliwell, 1992). However, the effect of very short and ultrashort-wavelength X-rays needs further investigation. With high transmission of X-rays as in high-pressure studies with ultrashort wavelength, the intensity of a Bragg reflection for a given absorbed energy in the sample is practically independent of the wavelength (Arndt, 1984). However, it is not known whether radiation damage in the crystal follows the energy dose absorbed or the number of absorbed photons.

2.1.2. Quasi-plane wave. When using a DAC and ultrashort wavelength, two requirements must be satisfied simultaneously: the X-ray beam must be tightly collimated in order to avoid diffraction by the metal gasket encapsulating the crystal and to allow exposures of several zones of the crystal and the size of Bragg spots on the detector must be as small as possible despite the large crystal-to-detector distance D (at the selected wavelength, D = 0.60–1.5 m for a detector with a circular sensitive area of diameter 0.3 m). The solution is a parallel beam instead of a beam focused either on the crystal or on the detector as in standard data collection. Further, the combination of parallelism and narrow bandpass has various effects which contribute to improve the signal-to-noise ratio and overall data quality.

(i) The very high angular resolution is ideal for the study of crystals with large unit-cell parameters.

(ii) The intrinsic angular width of Bragg reflections from macromolecular crystals, which is often extremely narrow at room temperature (Fourme *et al.*, 1995), is preserved.

(iii) The parameters (δx, δy, $\delta\omega$) of integration boxes around Bragg spots depend on the sample characteristics, without significant broadening owing to instrumental effects.

(iv) The probability of perturbation of diffracted intensities by the (few) Bragg reflections from diamonds is very low because Bragg reflections from both the diamonds and the crystal are very narrow.

(v) Energy filtering by the imaging plate near the Ba K absorption edge (as described previously) is more effective at low resolution because the edge profile is minimally broadened by instrumental effects.

In our experiments, an Si(111) double-crystal monochromator ($\delta\lambda/\lambda = 1.4 \times 10^{-4}$) was used without any focusing optics.

2.1.3. High intensity. In the rotation geometry, the λ^2 dependence of an integrated diffraction spot (Arndt, 1984) implies a reduction of scattering power by one order of magnitude from 1 to ∼0.3 Å. This penalty can be compensated with a high-brilliance X-ray source, such as undulators inserted in a high-energy storage ring such as ESRF. Our experiments were carried out at ID30 with two collinear undulators U40 and U35 (*i.e.* with magnetic periods of 40 and 35 mm, respectively). These devices will be replaced in 2004 by a pair of U23 phased undulators which will reduce exposure times by nearly one order of magnitude. With these extremely powerful sources, the use of a monochromator with a smaller bandpass such as Si(311) ($\delta\lambda/\lambda = 2.9 \times 10^{-5}$) might be considered.

2.2. Detector

The most important features of the detector are a 'reasonable' DQE at ultrashort wavelength, a large surface, a small point-spread function (PSF), a low detector noise and a fast readout. All these characteristics are important with respect to the data-collection efficiency, as defined later.

With reasonable DQE and low detector noise, fewer photons are required, which reduces radiation damage with a given statistical accuracy (note that DQE values at ultrashort wavelengths for relevant detectors such as CCD, imaging plates and amorphous selenium panels are not well documented).

Both large surface and small PSF increase the signal-to-noise ratio. For a given wavelength, the background level varies as D^{-2}, whereas the cross-section of the diffracted beams is nearly independent of D when using a quasi-plane wave. In the case of sharp spots as obtained with our setup, the small PSF would be quite effective, allowing the use of smaller integration boxes on the detector. Detectors based on a flat amorphous selenium panel have attractive characteristics in this respect (J. Hendrix, private communication). Finally, a fast readout (in the 1 s range) reduces the migration of radicals produced by irradiation in the unexposed zones of the sample.

2.3. Sample preparation and data collection

Inconel gaskets were prepared as described by Fourme *et al.* (2001). The cavity machined by electro-erosion in each gasket was cylindrical (diameter ≃ 300 µm) and the thickness was ∼200 µm after indentation. The beam was collimated by slits to 40–60 µm in both directions. During data collection, the sample was translated every few frames, typically by 40 µm, in order to irradiate fresh zones. Reflections were indexed and

integrated using *DENZO* (Otwinowski & Minor, 1997), with data from each zone treated as a block. In the *DENZO* command file, the value of a rejection parameter called SLOPE (the slope of the background plane above which the entire background and spot are considered unacceptable and rejected) was set to 110 instead of 50 (the default value) for successful integration. $R_{\rm full}$ (defined in Table 1) increases gradually in a series of frames collected on the same zone as a consequence of radiation damage. Frames with $R_{\rm full} > 0.4$ for the last resolution shell were rejected. Finally, useful data from the various zones were rescaled and merged using *SCALA* (Collaborative Computational Project, Number 4, 1994).

Table 1
HP data collection.

Results of data analysis from the program *SCALA* (Collaborative Computational Project, Number 4, 1994) are shown with the breakdown in resolution shells. $R_{\rm sym}$ is defined as $\sum_{hkl}\sum_{j=1,N}|I_{hkl}-I_{hkl}(j)|/\sum_{hkl}NI_{hkl}$. $R_{\rm full}$ is the $R_{\rm sym}$ factor for fully recorded reflections in the relevant shell, $R_{\rm cum}$ is the cumulative $R_{\rm sym}$ for all reflections, $N_{\rm meas}$ is the number of measured reflections and $N_{\rm ref}$ is the number of unique reflections. There were 370 600 measured reflections, including 238 288 (64.2%) fully recorded reflections and 132 312 partially recorded reflections. 3277 reflections (0.9%) were rejected. The large fraction of fully recorded reflections reflects the low mosaicity of samples. Note also the high completeness up to the last shell. The relatively high $R_{\rm full}$ values in the second and third resolution shells are a consequence of the low average intensity in these shells associated with the capsid structure.

$1/d^2$	$d_{\rm min}$ (Å)	$R_{\rm full}$ (%)	$R_{\rm cum}$ (%)	Average I	$\sigma(I)$	$I/\sigma(I)$	$N_{\rm meas}$	$N_{\rm ref}$	Completeness (%)	Multiplicity
0.0128	8.84	5.7	6.1	1883	166	11.3	11328	3021	89.0	3.3
0.0256	6.25	10.4	8.9	1130	174	6.5	21950	5586	91.2	3.5
0.0384	5.10	10.8	10.2	1301	209	6.2	28712	7251	91.0	3.5
0.0512	4.42	8.1	9.5	2184	261	8.4	33668	8594	91.4	3.5
0.0640	3.95	8.9	9.6	2097	277	7.6	38248	9710	91.6	3.5
0.0768	3.61	12.0	10.3	1525	271	5.6	42471	10715	92.0	3.5
0.0896	3.34	15.4	11.3	1223	274	4.5	46395	11747	92.2	3.5
0.1023	3.13	20.4	12.5	904	271	3.3	49546	12536	91.8	3.5
0.1151	2.95	25.9	13.8	700	263	2.7	51586	13208	92.0	3.4
0.1279	2.80	34.4	14.9	487	242	2.0	46696	12837	88.6	3.1
Overall		13.8	14.9	1248	254	4.9	370600	95205	91.2	3.4

3. Results of data collection on cubic CPMV crystals

Cubic CPMV crystals grown under previously published conditions (Lin *et al.*, 1999) exhibit polymorphism. About 10% of the rhombic dodecahedral CPMV crystals conform strictly to the characteristics of the cubic *I*23 space group and diffract to high resolution. The other crystals have weak reflections with indices $h + k + l = 2n + 1$ (odd reflections) which should be absent in the body-centred space group. The intensities of odd reflections vary from one crystal to another and the variation of the average diffracted intensity as a function of resolution is abnormal. The crystals with odd reflections diffract X-rays poorly compared with those conforming to the strict *I*23 space group. The space group *P*23 was tentatively assigned to poorly diffracting crystals, which agreed with the presence of odd reflections but not with the packing criteria of the virus particles. The current interpretation is that the orientation of virus particles in the *P*23 structure deviates randomly from the standard orientation in space group *I*23 (Schildkamp *et al.*, 2003). The polymorphism is a complication in crystallographic studies on CPMV and its mutants, as many crystals are required for screening for a few suitable for data collection (T. Lin & J. E. Johnson, private communication).

3.1. Data collection at 295 K and 330 MPa

A total of eight crystals with the rhombic dodecahedral morphology and edges of about 170 µm were employed in the high-pressure study. A stabilization solution (32% MPD, 200 m*M* ammonium sulfate, 3% PEG 800 and 50 m*M* potassium phosphate buffer pH 7.0) was used as the compression medium. The ramping rate was about 10 MPa min^{-1} until 330 MPa was reached. All diffraction patterns collected below 200 MPa could only be indexed in the *P*23 space group, showing diffraction to modest resolution (4–5 Å) and poor mosaicity (∼0.3°). A structural transition occurred beyond 200 MPa, with a spectacular improvement in resolution. The diffraction patterns could now easily be indexed in the cubic *I*23 space group, with a mosaicity as small as 0.03° on some fresh samples. This transition is reversible with the release of pressure. These results confirm and consolidate our preliminary findings (Fourme *et al.*, 2002). The largest number of useful frames collected on a single zone was 11. Finally, we merged a total of 370 600 measured reflections, which led to a set of 95 205 unique reflections (HP data set) with 91.2% completeness at 2.8 Å resolution [defined on the basis of $I/\sigma(I)$ cutoff ≥ 2]. The data collection is summarized in Table 1. Parameters for data acquisition are given in Table 2.

3.2. Data collection at 279 K and atmospheric pressure

We used as a reference a data set collected several years ago at beamline F1 at CHESS (Cornell University; Lin *et al.*, 1996), which is probably the best set ever collected at atmospheric pressure with CPMV, at least at or near room temperature.[2] Six crystals about of 1 mm edge, conforming strictly to space group *I*23, were selected. Each sample was translated several times in order to irradiate fresh zones, with the beam collimated to 100 × 100 µm. The parameters for data acquisition are given in Table 2. Merging the collected data gave 104 978 unique reflections (AP data set), with ∼100% completeness at 2.8 Å resolution [defined on the basis of $I/\sigma(I)$ cutoff ≥ 4].

3.3. Data-collection efficiencies

High-pressure (HP) and atmospheric pressure (AP) data were acquired from *I*23 CPMV crystals under very different experimental conditions (sample volume, pressure, wave-

[2] Better data have been collected at the APS (Chicago) on cryocooled crystals (T. Lin, private communication), but are not relevant here as high-pressure studies are performed at room temperature.

Table 2
Specifications and parameters for CPMV data collection at 279 K and atmospheric pressure at CHESS and 295 K and 330 MPa at ESRF (AP and HP sets, respectively).

For the AP set, the useful angular ranges were multiplied by four with respect to the experimental values in order to define the resolution on the basis of $I/\sigma(I)$ cutoff ≥ 2 in both sets (see main text). Mosaicity is defined according to the *DENZO* model and includes instrumental effects. 'Useful' range means that data collected in this range reach or exceed the target resolution [here, 2.80 Å at $I/\sigma(I)$ cutoff ≥ 2]. For each set, the DCE value is based on the zone which provided the largest useful angular range.

	AP	HP
Common specifications and parameters		
Beamline	CHESS F1	ESRF ID30
Energy of stored electrons (GeV)	5	6
Equivalent intensity (mA)	200	180
Source	24-pole wiggler	Undulator
Detector	Fuji IP (BAS 2000)	Fuji IP (MAR 345)
X-ray optics	Bent Si(111), bent mirror	Flat Si(111), mirror removed
Wavelength (Å)	0.908	0.331
Beam cross-section (µm)	100 × 100	50 × 50
Beam divergence (µrad)	600	5 (V) × 25 (H)
Oscillation angle per frame (°)	0.3	0.3
Exposure time per frame (s)	15	80
Crystal-to-detector distance (mm)	400	1375
Parameters for the crystal and zone selected for the calculation of data-collection efficiency		
Crystal size (µm)	∼1000 × 1000 × 1000	∼170 × 170 × 170
Unit-cell parameter (Å)	317	313.9
Initial mosaicity (°)	0.080	0.045
No. of irradiated zones	9	3
Volume of irradiated zone (µm)	∼100 × 100 × 1000	∼50 × 50 × 170
Total useful angular range (°)	18	7.2
Largest angular range acquired per irradiated zone (°)	2.4	3.3
DCE for this zone (° mm^{-3})	240	7764
Relative DCE	1	32

length and divergence of the X-ray beam, signal-to-noise ratio *etc*.). We tried to address the following question: what is the set of conditions which 'took the best' from a given sample; that is, which provided the highest data collection efficiency (DCE)? Here, efficiency is related to the information content acquired per unit volume of crystal. In order to make a meaningful comparison, the prerequisite is that the information content in the data sets to be compared should be nearly identical, a condition which translates into similar completeness and signal-to-noise [*i.e.* the same resolution for a given $I/\sigma(I)$ cutoff].

The ratio of the total diffracting volumes required to acquire a high-completeness data set at a given resolution might be used to compare the efficiencies. Instead, we suggest a simple operational definition of DCE based on a selected subset of data and therefore unbiased by the particular course and variations of a full data collection. It is defined as $\Delta\omega/\Delta\tau$, where $\Delta\omega$ is the angular range through which useful data can be acquired from a zone of the crystal and $\Delta\tau$ is the volume of the zone bathed by the X-ray beam. In order to obtain the practical upper limit of DCE for a set of experimental conditions, it is calculated for the particular zone which provided the largest number of useful frames in the data set. Comparing DCE for different experimental conditions does not require that crystals have the same orientation on the goniometer head, unless diffraction is strongly anisotropic.

To compare DCE for the AP and HP sets (Table 2), information contents were approximately equalized. Both sets have a completeness in excess of 91%. Signal-to-noise ratios would be identical [2.8 Å resolution on the basis of $I/\sigma(I)$ cutoff ≥ 2] if the AP set had been recorded with exposure times four times shorter, which would have increased the useful angular ranges by about the same factor. Accordingly, the useful angular ranges for the AP set in Table 2 are the experimental values multiplied by four.

Table 2 shows that the DCE is higher for the HP case. The gain is such that this conclusion is independent of the large relative uncertainties in the $\Delta\omega$ and $\Delta\tau$ values (estimated to about 20 and 30%, respectively). It is important to note that in our experiments on CPMV crystals, many parameters are involved in the improvement of DCE and it is difficult to assess the particular role of one of them. For instance, it would be premature to conclude from our results that ultrashort wavelengths increase the sample lifetime.

4. Conclusions

These results demonstrate that it is technically possible to acquire high-pressure diffraction data from a complex macromolecular assembly with the quality required for structural studies. As in the case of tetragonal hen egg-white lysozyme (Fourme *et al.*, 2001), both the high-symmetry space group of the CPMV crystals and their isotropic shape were favourable for the acquisition of a highly complete data set using few crystals. Diamond cells with larger angular apertures will be more suitable for studying crystals either in lower symmetry space groups or with very anisotropic shape (*e.g.* platelets, which tend to align with their large faces parallel to diamond culets).

The higher efficiency of the HP data collection is based on the multifaceted improvement in signal-to-noise provided by the particular experimental conditions. A similar strategy can be applied in conventional data collection (*e.g.* without a high-pressure cell, on crystals at room temperature or cryocooled) as a step toward the measurement of 'ideal data' based on the higher brilliance at much shorter wavelengths than hitherto available (Helliwell, 1992; Helliwell *et al.*, 1993). The gain in signal-to-noise ratio will be of particular interest for difficult problems including small, radiation-sensitive and poorly diffracting samples and very high resolution data collection. Another benefit would be to reduce systematic errors and increase the internal consistency of data for the exploitation of small anomalous signals for phasing at a single wavelength (SAD). Systematic experiments optimized in every respect for high DCE, including the use of a quasi-plane wave of ultrashort wavelength, should be undertaken on samples both at room and cryotemperatures. On this basis, the usefulness of new purposely designed macromolecular-crystallography beamlines could be assessed.

The support of the ESRF staff, in particular on the ID30 beamline, was greatly appreciated. We thank Andrew Thompson at Synchrotron SOLEIL for useful comments and suggestions.

References

Arndt, U. (1984). *J. Appl. Cryst.* **17**, 118–119.
Collaborative Computational Project, Number 4 (1994). *Acta Cryst.* D**50**, 760–763.
Fourme, R., Ascone, I., Kahn, R., Mezouar, M., Bouvier, P., Girard, E., Lin, T. & Johnson, J. E. (2002). *Structure*, **10**, 1409–1414.
Fourme, R., Ducruix, A., Riès-Kautt, M. & Capelle, B. (1995). *J. Synchrotron Rad.* **2**, 136–142.
Fourme, R., Kahn, R., Mezouar, M., Girard, E., Hoerentrup, C., Prangé, T. & Ascone, I. (2001). *J. Synchrotron Rad.* **8**, 1149–1156.
Gonzalez, A., Denny, R. & Nave, C. (1994). *Acta Cryst.* D**50**, 276–282.
Helliwell, J. R. (1992). *Macromolecular Crystallography with Synchrotron Radiation.* Cambridge University Press.
Helliwell, J. R., Ealick, S., Doing, P., Irving, T. & Szebenyi, M. (1993). *Acta Cryst.* D**49**, 120–128.
Helliwell, J. R. & Fourme, R. (1983). *The ESRF as a Facility for Protein Crystallography: a Report and Design Study.* Geneva, Switzerland: CERN.
Katrusiak, A. & Dauter, Z. (1996). *Acta Cryst.* D**52**, 607–608.
Kundrot, C. E. & Richards, F. M. (1986). *J. Appl. Cryst.* **19**, 208–213.
Kundrot, C. E. & Richards, F. M. (1987). *J. Mol. Biol.* **193**, 157–170.
Lin, T., Chen, Z., Usha, R., Harrington, M., Schmidt, T. & Johnson, J. E. (1999). *Virology*, **265**, 20–34.
Lin, T., Porta, C., Lomonossoff, G. P. & Johnson, J. E. (1996). *Folding Des.* **1**, 179–187.
Otwinowski, Z. & Minor, W. (1997). *Methods Enzymol.* **276**, 307–326.
Schildkamp, W., Lin, T. & Johnson, J. E. (2003). In preparation.
Schiltz, M., Kvick, A., Svensson, O. S., Shepard, W., de La Fortelle, E., Prangé, T., Kahn, R., Bricogne, G. & Fourme, R. (1997). *J. Synchrotron Rad.* **4**, 287–297.
Urayama, P., Phillips, G. N. & Gruner, S. M. (2002). *Structure*, **10**, 51–60.
Van Valkenburg, A. (1962). *Rev. Sci. Instrum.* **33**, 1462.
Weir, C. E., Lippincott, E. R., Van Valkenburg, A. & Bunting, E. N. (1959). *J. Res. Natl Bur. Stand. A*, **53**, 55–62.